Artigo

MODIFIED MAGNETITE NANOPARTICLES WITH THE JUICE OF PLANTAIN PSEUDOSTEM: AN OPTION FOR WATER DECONTAMINATION

Camilo Eduardo García Henao[a], Guillermo Salamanca Grosso[b], Hoover Albeiro Valencia Sánchez[c] and Anderson Guarnizo Franco[b,*]

[a]Programa de Química, Universidad del Quindío, 630001 Quindío, Armenia, Colombia
[b]Departamento de Química, Universidad del Tolima, 730006299 Ibagué, Tolima, Colombia
[c]Facultad de Tecnología, Universidad Tecnológica de Pereira, 660003 Pereira, Risaralda, Colombia

Recebido em 12/05/2023; aceito em 04/08/2023; publicado na web 12/09/2023

In recent years, various methods for surface functionalization of magnetite nanoparticles with emerging modifications have been explored and reported. Green nano-chemistry aims to synthesize nanomaterials using bio-based resources, providing new materials for biological and environmental applications. Surface modification of magnetite nanoparticles using phytochemicals extracted from plants is a fundamental principle of green synthesis routes. Agricultural waste from different crops, such as plantain pseudostem, is of particular interest as a renewable resource due to its abundant availability, low toxicity, and economic feasibility. In this study, the juice extracted from plantain pseudostem was utilized for the phytofunctionalization of magnetite nanoparticles. Characterization techniques including transmission electron microscopy (TEM), scanning electron microscopy (SEM), thermogravimetric analysis (TGA), and fourier-transform infrared spectroscopy (FTIR) confirmed the nanometric dimensions of the composite (size range of 12.6 ± 3.17 nm) and established its organic-inorganic nature. The superparamagnetic properties of the composite were also demonstrated. Moreover, the potential application of this nanohybrid in bioremediation for the immobilization of cadmium(II) and lead(II) showed promising results, highlighting its efficacy in managing water pollutants.

Keywords: green chemistry; biofunctionalization; bioremediation; phytofunctionalization; natural products; nanotechnology.

INTRODUCTION

Metal and oxide nanoparticles (NPs) have been extensively engineered to create composite materials with diverse applications in fields such as medicine, engineering, environmental sciences, electronics, and power supply. NPs, which typically range in size from 1 to 100 nm,[1,2] can be tailored to incorporate both inorganic and organic components, allowing for the design of functional materials.[3,4] This versatility of NPs expands the possibilities for developing hybrid organic-inorganic nanomaterials with unique properties. Magnetite nanoparticles (Fe_3O_4 or MNPs), in particular possess biocompatibility, stability, superparamagnetism, and chemical versatility, making them highly desirable for various technological applications.[5]

However, the production of some nanostructured composites involves the use of toxic solvents, the generation of hazardous by-products, reliance on non-renewable sources, and high power consumption.[6] Addressing these concerns requires the development of environmentally friendly protocols for the manufacture of nanocomposites.[7-9] A promising approach is the utilization of renewable natural resources as raw materials in the design and synthesis of nanomaterials, as demonstrated in several studies (Table 1). Phytochemicals extracted from plants and incorporated into metal NPs without significant treatments to modify them, have shown to be a smart way to meet to green chemistry principles.[10-12] Phytochemicals derived from various plant parts, including leaves,[13] fruits,[14] stems,[15] roots,[16] exudates,[17] peels,[18] and seeds[19] have been used to modify the NPs through covalent or ionic linkages to the metal atoms that are present at the surface in a strategy called phytofunctionalization.[20]

Biobased nanomaterials have been extensively developed for a wide range of innovative applications, as summarized in Table 1. These applications encompass the effective removal of traditional organic pollutants like benzene, as well as emerging organic pollutants such as pharmaceuticals (*e.g.*, ibuprofen). Additionally, biobased nanomaterials have demonstrated promising potential for antibacterial applications and the efficient removal of heavy metals from various sources.

One of the key advantages of these materials is their high specific surface area, which enables enhanced adsorption capabilities. Moreover, they possess excellent dispersibility in water, allowing for easy handling and application. The incorporation of magnetic properties in these nanomaterials enables convenient recovery using external magnetic fields. Additionally, their chemical versatility allows for tailored modifications to achieve desired properties and functionalities. However, it is important to note that typical and bio-based adsorbents can also have certain limitations. The synthesis of support materials or the adsorbent layer can be time-consuming, and the production process may be costly. Furthermore, the generation of toxic by-products during synthesis can be a concern. These aspects need to be considered and addressed when developing and utilizing these materials for practical applications.

Colombia is a well-known producer of *Musaceae* species that includes plantain (*plátano*), *cachacho*, *bocadillo*, and bananas.[29] Plantains hold cultural significance in the Andina region from this country and are widely used as a traditional ingredient in gastronomy. Roughly, this plant consists of leaves, fruits, a pseudostem, and roots (Figure 1). After the fruit (plantain) is harvested, the leaves and pseudostem are typically discarded as residual material, used as biofertilizer, or incinerated.[30,31]

In a preliminary study,[32,33] it was found that the pseudostem comprises a fibrous fraction and a liquid component known as pseudostem juice (PS). Phenolic compounds were detected in a PS sample using tests with ferric trichloride, lead acetate, and Foling-Ciocalteu reagent. The *Musa* sp. genus, to which plantains

*e-mail: aguarnizof@ut.edu.co

Table 1. Uses of bio-based nano-materials in water decontamination

Nanomaterial	Bioresource	Pollutant	Advantages	Disadvantages
GO-Fe_3O_4[21]	Graphene oxide (GO) from graphite and decorated with nano-magnetite	Hydrochlorothiazide with a 67.86% removal of the contaminant at pH 7.0	High specific area, hydrophilicity, thermal and chemical stability, high affinity by organic pollutants, easy to manipulate by external magnetic field	Time-consuming synthesis, undesirable by-products as Mn species during GO synthesis
Fe_3O_4@EUG[22]	Magnetite synthesis from a eugenol (EUG) aqueous solution	Antibacterial: *S. aureus* *P. aeruginosa* *E. coli* *E. faecalis*	Less toxicity than free eugenol in healthy cells; Biocompatibility	Free eugenol showed better antimicrobial properties
CT-Fe_3O_4[1]	Chitosan (CT) decorated with MNPs	Methotrexate (MTX)	All the nanohybrids presented better MTX adsorption properties than magnetite or chitosan	At pH 7 the CT-Fe_3O_4 1:1 was able to remove less than 30% of the MTX initial amount
Fe_3O_4@OA[23]	MNPs stabilized with oleic acid (OA) under microwave radiation	Benzene	Highest adsorption capacity at neutral pH (77.1 mg g^{-1}); Improved adsorption properties than non-nanostructured OA	It is necessary to use methanol to recover a significant part of the adsorbed benzene
Fe_3O_4@PB[24]	MNPs stabilized with pine bark (PB)	Levofloxacin Trimethoprim	Optimal adsorption of both pollutants at the 6.5-7.5 pH range; The usage of pine bark is in favor of the circular economy	Irregular size of MNPs from 1 nm to bulk; A possible variation on the pine bark composition by chemical reaction prompted by MNPs
HAP@CT@Fe_3O_4[25]	Hydroxyapatite (HAP) and chitosan (CT) as support of MNPs	Deflazacort (DEF) Ibuprofen (IBU) Methylprednisolone (MET) Norfloxacin (NOR)	Adsorption is not pH dependent (except for NOR with the highest adsorption rate at pH 7)	It is necessary to use a slightly acidic solution to achieve a high desorption rate; Lack of material structure understanding as the magnetic behavior
Fe_3O_4@PTh[26]	Polythiophene (PTh) onto MNPs	Nitrobenzene	Higher adsorption capacity than other reported materials; The material showed stability after several recuse cycles (10)	Some time-consuming previous synthesis steps of PTh
Fe_3O_4@SiO_2/PA(G1)-Mu Fe_3O_4@SiO_2/(G2)-Mu[27]	The magnetite was modified with SiO_2 and one and two generations (G) polyamidoamine (PA) dendrimers linked to murexide (Mu)	Lead(II)	Highest efficiency at pH 5 for both materials; Better performance than other reported materials	Several steps synthesis leading to higher costs, time consuming and waste generation
Fe_3O_4@HA[28]	Humic acid (HA) supported on MNPs	Methylene blue	High adsorption capacity of (161.290 mg g^{-1}); The developed nanohybrids exhibited better adsorption performance than humic acid itself; There were no significant structural changes on the material after the adsorption cycles	No superparamagnetic material; Nano-size did not demonstrate

belong, is recognized as a source of various phenolic compounds such as flavonoids, anthocyanins, catechins, tannins, and condensed tannins.[34-36] These phenolic compounds possess intrinsic properties such as chelating capability, hydrogen bonding, pH responsiveness, redox potentials, radical scavenging, polymerization, and light absorbance, which makes them a distinct class of structural motifs for the synthesis of functional materials.[37]

Based on the available literature,[35,38-40] we hypothesized that the PS juice could serve as a valuable source of phenolic compounds and potentially be used as a capping agent in the modification of MNPs. In a previous study by Venkateswarlu *et al*.,[41] an extract of peels from an unknown banana specie, was used to obtain a nanohybrid with MNPs. However, their resulting product exhibited ferromagnetic behavior instead of the desired superparamagnetic properties. Upon analyzing the images of the NPs synthesized by the Venkateswarlu team, we concluded that their size exceeded 30 nm and the polydispersity of the NPs was responsible for the observed magnetic behavior.[5]

Furthermore, these researchers did not explore a practical application of their nanohybrid. To overcome these limitations, we propose an alternative synthesis route to obtain a new superparamagnetic hybrid material using an identified plantain species. To conceptualize a green synthesis route, we considered

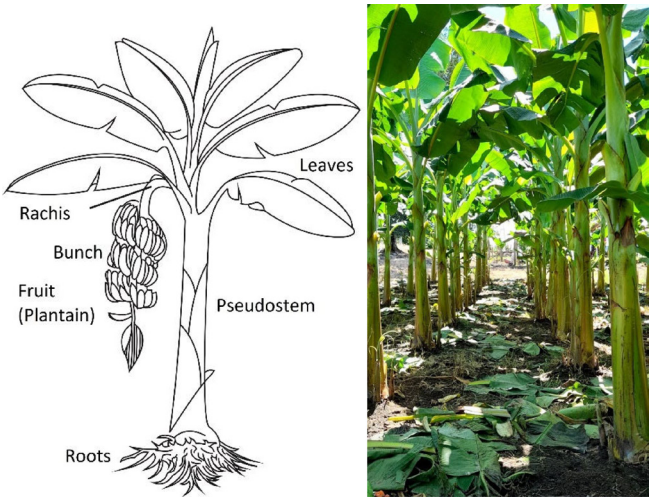

Figure 1. *Left: plantain plant scheme. Right: plantain farming at "La colombina" (picture: López, C.)*

the prior synthesis of bare MNPs, utilizing MNPs as a scaffold for biomolecules, utilizing PS juice for phytofunctionalization of MNPs without additional treatment, employing a sonochemical route for synthesis, and excluding the use of toxic organic solvents. These considerations enabled us to develop a green and environmentally friendly approach for synthesizing the superparamagnetic nanohybrid material, with potential for capturing heavy metals present in water.

In this study, we have successfully synthesized a biobased material designed for the removal of heavy metals from aqueous media. By utilizing PS phytochemicals, we offer an alternative solution to address the inherent chemical instability often encountered with magnetic nanoparticles (MNPs). This innovative nanocomposite overcomes the limitations associated with conventional adsorbents, which typically require additional filtration and centrifugation steps in decontamination processes.

Therefore, considering the anticipated excellent properties of the developed material, this study introduces a green synthesis strategy that utilizes water as the sole solvent throughout the entire synthesis process. This approach not only eliminates the need for additional toxic reagents but also promotes an environmentally friendly application. Additionally, the magnetic manipulation of the hybrid material simplifies the process of pollutant removal, leading to time-saving operations in decontamination processes. Furthermore, by harnessing the abundant availability of phytochemical resources, the nanomaterial effectively avoids the reliance on exotic and costly reagents. Overall, this eco-friendly approach showcases the potential for sustainable and cost-effective solutions in the field of pollutant removal and environmental remediation.

EXPERIMENTAL PART

All the reagents were purchased from Aldrich in "for synthesis" quality and were used without additional purification. The deionized water was done by using a Millipore Helix 3 device. The separation assisted by an external magnetic field was made with a neodymium magnet ($Nd_2Fe_{14}B$).

Pseudostem juice (PS) obtention

Pseudostem (*Musa paradisiaca* var. Domico hartón) came from farm "La colombina", located at the Caicedonia town (Valle del Cauca, Colombia), at 4°22'9" N 75°52'34", and 1180 m of altitude. Pseudostem was collected when their fruit (plantain) was harvested. After that, 300 g of pseudostem was crushed in a blade mill (20000 rpm, 5 min) and the liquid fraction was filtered through a canvas cloth (*c.a.* 0.3 mm mesh) to remove insoluble solids, bubbled with nitrogen for 5 min at 3 mL min^{-1}, and was kept for 24 h at 4 °C under nitrogen. This cold juice was centrifuged at 1000 rpm for 10 min, decanted, and filtered through filter paper free of ashes, the later liquid obtained (PS) was then bubbled with nitrogen for 30 min at 3 mL min^{-1} to air exclusion. This product was used as stabilizing as well as a modification agent of magnetite nanoparticles. Besides, 100 mL of PS was dried under low pressure at room temperature and the solid was stored under nitrogen for further analysis.

UV/Vis measurement was made in a Genesys 10S-UV/Vis spectrophotometer from Thermo Scientific. Phenolic compounds were estimated by the referenced spectrometric UV/Vis method (Folin-Ciocalteu).[42-44] Briefly, a linear plot was performed from 1.00 mg L^{-1} to 20.00 mg L^{-1} from a stock solution (1000 mg L^{-1}) of tannic acid. The samples were mixed with 0.5 mL of Folin-Ciocalteu solution, 1.00 mL of a 20% w/v $NaCO_3$ solution, then water was added to complete 10.00 mL. The obtained samples were incubated in dark for 2 h before the read of their absorbances at 725 nm. The total phenolic content was expressed as tannic acid equivalent (TAE) in mg L^{-1}.

Synthesis of modified magnetite NPs using PS

First, bare magnetite NPs (Fe_3O_4) were synthesized by the typical coprecipitation method.[45] Under nitrogen, a mixture of iron(II) sulfate heptahydrate (6.95 g, 25.25 mmol) and iron(III) sulfate (10.00 g, 258.78 mmol) was dissolved in deionized water (250 mL). Next, 25% w/v of ammonia solution was added to reach a pH of 10. This mixture was then kept for 1 h at 50 °C. After that, the solid collated with the aid of a neodymium magnet was rinsed with deionized water (3 × 30 mL), and acetone (3 × 30 mL). Afterward, the solid (Fe_3O_4@PS) was vacuum dry for 2 h and stored under nitrogen at 4 °C.

Secondly, the process of surface modification of MNPs was accomplished by the sonochemical method. Briefly, under nitrogen, 400 mg of MNPs were dispersed in 20 mL of deionized water in an ultrasonic bath (40 kHz) Derui brand. Next, 30 mL of PS was poured, then the reaction mixture was incubated in an ultrasonic bath for 1 h. At the end of that period, the Fe_3O_4@PS were magnetically gathered, washed with deionized water (3 × 30 mL) and ethanol (3 × 30 mL), and finally, before vacuum drying, the Fe_3O_4@PS nanohybrid was preserved at 4 °C under nitrogen for further analysis. Dry PS, as well as MNPs, were used as control. Also, water and PS mix without MNPs was treated by ultrasonic waves as a control test.

All the experiments were carried out at least in triplicates and representative data are presented here.

Characterization

Magnetic measures were made in a SQUID magnetometer from Quantum Design MPMS XL. The samples do not require previous preparation.

For electronic transmission microscopy (TEM) a JEOL 2100 with a LaB6 of 200 kV thermionic beam was used. The solid samples were dispersed in ethanol and fixed via drop-casting onto 200 mesh carbon-coated copper grids. The electronic scanning microscopy images were obtained with a Leica -Zeiss LEO 440 microscope after the samples were fixed on an aluminum specimen mount stub by drop-casting with ethanol as solvent. For size distribution determination (size (nm) ± *s*), 500 NPs were randomly selected, and their diameter was determined.

Fourier transform infrared spectroscopy was achieved in a Nicolet Impact 400 FT-IR spectrometer. The sample was crushed

with potassium bromide (KBr) powder and pressed to conform to a solid disc before FT-IR analysis. A pure KBr disc was used for background correction.

Some samples were analyzed by thermogravimetric analysis (TGA). About 10 mg of sample were decomposed in a Mettler-Toledo TGA 851; nitrogen flux was kept at 50 mL min^{-1}, and temperature *versus* mass loss was registered from 30 °C up to 1000 °C, in a 10 °C min^{-1} of the gradient. Also, the first derivative of TGA (DTGA) was plotted.

Chelating activity

Chelating activity is based on the concentration measurements of some dissolved metals in water before and after the treatment with an adsorbent.[46-48] In this paper, the chelating activity was made by mixing 10 mg de Fe_3O_4@PS with 20 mL of cadmium(II) and lead(II) solutions of 10, 30, 50, 100 and 200 mg L^{-1}, both prepared separately from $Cd(NO_3)_2$ and $Pb(NO_3)_2$. After continuous agitation within 6 h, the Fe_3O_4@PS was gathered by an external magnet, and the liquid fraction was separated for atomic absorption analysis (AA) of Cd and Pb in an Analitik Jena spectrometer model ZEEnit 700P. The concentration of metal ions in the solution was determined according to the APHA method.[49] The results were expressed as % of removed metal from the original solution.

The metal absorption capability (q_e) (mg g^{-1}) was calculated as follows (Equation 1):

$$q_e = \frac{(C_0 - C_e) \times V}{m} \quad (1)$$

were C_0 and C_e (mg) are the initial amount of metal ion and the amount of metal ion unadsorbed in the solution at the equilibrium time (q_e), respectively. V is the volume of the Pd(II) and Cd(II) ion solution (L) and m is the mass of nanocomposite (g). Percentual removal of metal refers by Equation 2:

$$\text{Removal}(\%) = \frac{(C_0 - C_e)}{C_0} \times 100 \quad (2)$$

The Langmuir isotherm linear (Equation 3)[50] was used to compare the adsorption capability of the Fe_3O_4@PS with those from literature.

$$\frac{C_e}{q_e} = \frac{1}{K_L q_m} + \frac{1}{q_m} C_e \quad (3)$$

were K_L is the Langmuir constant or sorption coefficient (L mg^{-1}) and q_m is the maximum amount of metal ions required to form a monolayer (mg g^{-1}).

RESULTS AND DISCUSSION

Synthesis and characterization of Fe_3O_4@PS

The liquid fraction of plantain pseudostem (PS) was determined to have a tannic acid equivalent (TAE) of 241.00 ± 1.03 mg L^{-1}, both with and without ultrasound treatment, indicating that ultrasound treatment did not significantly alter the TAE value. However, when magnetite nanoparticles (MNPs) were dispersed in the PS and subjected to sonochemical process, the TAE concentration decreased to 175.10 mg L^{-1}. This finding suggests that a portion of the phenolic compounds present in the PS was retained by the MNPs, as evidenced by the unchanged TAE concentration in the control test without MNPs. Additionally, it was observed that the black dispersed solid containing the MNPs exhibited magnetic properties, as it was attracted by a magnet. This observation indicates that the MNPs have the capability to absorb, degrade, or alter the original phenolic content of the PS. Based on these results, it was concluded that the MNPs effectively interacted with the phenolic compounds, resulting in a reduction in their concentration in the liquid fraction. Furthermore, the material obtained after ultrasonic treatment, which displayed magnetic responsiveness, was washed, isolated, and dried to obtain a black solid named as Fe_3O_4@PS. This solid material was kept for further studies.

Magnetic properties of Fe_3O_4@PS

The magnetic behavior of Fe_3O_4@PS was compared with that of bare MNPs by SQUID magnetometry. Hysteresis loop of magnetic material showing the important parameters which are saturation magnetization (M_s) it demonstrates the complete magnetizability of magnetic materials, remanent magnetization (M_r), it reflects the magnetic field that is produced by the magnet after the magnetizing field has been removed and, magnetic coercivity (H_c) characterizes the magnitude of the reverse field required to achieve demagnetization.[41]

The hysteresis loop observed in the magnetization plot of Fe_3O_4@PS was barely evident at room temperature (r.t.), indicating that the material had a low residual magnetism at zero field. Specifically, the residual magnetism was measured to be 2.85 emu g^{-1} (entry 10, Table 2). In contrast, bare MNPs exhibited no residual magnetism, as indicated by the measurement of 0.00 emu g^{-1}. This observation suggests that the incorporation of the PS phytochemicals onto the MNPs resulted in a reduced residual magnetism, potentially due to the surface modifications and interactions between the components of the hybrid material. This means that the superparamagnetic property is slightly altered by the plant biomolecules, in contrast they protect them from intraparticle interaction and make the nanoparticle magnetic core more stable against the environment. The magnetic saturation in the novel material (64.50 emu g^{-1}) is lower than the non-treated MNPs (73.3 emu g^{-1}). This observation is expected if it is assumed that a non-magnetic organic fraction is incorporated over the MNPs.[51]

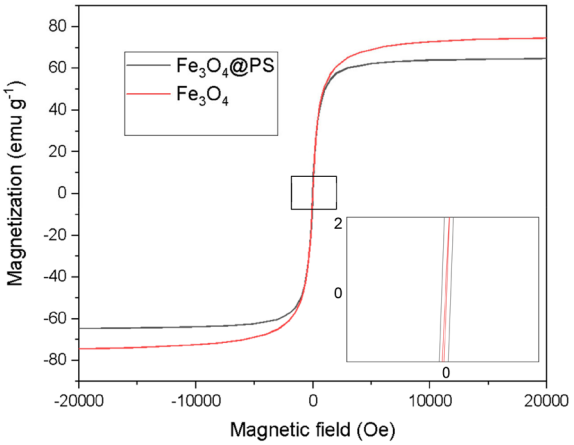

Figure 2. *Magnetization plot of MNPs and Fe_3O_4@PS at r.t.*

When compared to other bio-based magnetic nanoparticles (MNPs) listed in Table 2, Fe_3O_4@PS demonstrates excellent superparamagnetic properties. The superparamagnetic behavior is a crucial technical requirement for achieving easier dispersion, magnetic separation, and redispersion operations of the material in aqueous media. The recovery of the dispersed material becomes easier when the operation requires a less strong external magnetic

Table 2. Magnetic properties of some bio-based nanomaterials

Entry	Nanomaterial denomination	Bioresource	M_s (emu g^{-1})	H_C (Oe)	M_r (emu g^{-1})	Uses
1	Bare Fe_3O_4[52]	-	73.3	5.7	0.01	-
2	Fe_3O_4@Fritillaria/Pd NPs[53]	*Fritillaria imperialis* flower extract	42.5	n.r.	n. r.	Catalysis
3	CGFe_3O_4 NPs[54]	*Couroupita guianensis* fruit extract	0.11	48	0.10	Antibacterial
4	Fe_3O_4@BP[41]	Banana peel extract (specie unknown)	15.8	387.91	0.62	None
5	Fe_3O_4@CD[55]	Carbon dots by lemon and grapefruit extracts	34.0	5.00	0.00	*E. Coli* photoluminescence sensor
6	Fe_3O_4 MNRs[56]	Magnetic nanorods using *Punica granatum* rind extract decorated with MNPs	22.70	334.22	4.20	Removal of Pb(II) from aqueous solution
7	Fe_3O_4@nano-cellulose[57]	Nano-cellulose	36.71	5.13	0.19	Removal of radioactive ions from aqueous solution
8	Fe_3O_4@W. tea/Ag[58]	White tea extract (W. tea)	52.8	n.r.	n. r.	Catalysis
9	Fe_3O_4/*Thyme*-Cu[59]	Thymbra spicata flower extract	23.6	n.r.	n. r.	Antioxidant, cytotoxic
10	Fe_3O_4@PS	This work	64.50	18.12	2.85	Removal of Pb(II) and Cd(II)

n.r.: Not reported.

field, as indicated by the highest magnetization saturation in the list (64.50 emu g^{-1}) for Fe_3O_4@PS compared to 42.5 emu g^{-1} for Fe_3O_4@W. tea/Ag (Table 2, entry 8) as the best among the cited literature.

Infrared spectra and thermogravimetric analysis

The organic content could be inquired about by FT-IR. The PS juice is constituted by water-soluble carbohydrates, proteins, lipids, and phenolic compounds that may be participating as a capping agent in the process of nanoparticle modification in ultrasound treatment. The absorption spectrums of a vacuum-dried pure PS juice sample, MNPs, and Fe_3O_4@PS are depicted in Figure 3. The PS sample free water (dry PS) was a highly hygroscopic substrate, so care was advised for humid control when the FT-IR was developed.

In the FT-IR spectrums, there is a wide and intense band from 3650 to 2700 cm^{-1} representative of groups –OH tension in phenolic compounds as well as hydroxyl groups from the Fe_3O_4 surface.[60] C–H and CH_2 vibrations of aliphatic hydrocarbons are presented at 2915 cm^{-1}. The band at 1615 cm^{-1} is associated with carbonyl vibration of ketones, quinones, carboxylic acids, and esters in dry PS. In the same sample, the 1050 cm^{-1} band registers the C–O–C stretching vibration. The absorption peak observed around 1415 cm^{-1} is ascribed to C–OH aromatic stretching mode according to Karade *et al*.[61] Nevertheless, the group of signals from 1240 up to 1360 cm^{-1} can be indicative of amines since C–N vibration usually is observed in this segment. At 1627 cm^{-1} the hydrogens scissor bend vibration of and the wide one at 3500 cm^{-1}; it is plausible that some water molecules are strongly adsorbed in pure MNPs.[60] Pure magnetite spectrum and Fe_3O_4@PS, the intense band at 584 cm^{-1} is assigned to the IR active T_{1u} mode corresponding to the vibration of the Fe^{2+}–O^{2-} group.[62] The FT-IR results indicate consistent differences between the pure MNPs and the Fe_3O_4@PS, which means that PS provides capping molecules.

The thermal degradation behavior of Fe_3O_4@PS was investigated, revealing the presence of volatile organic components. Thermogravimetric analysis (TGA) and differential thermogravimetric analysis (DTGA) plots of Fe_3O_4@PS and pure magnetite nanoparticles (MNPs) are presented in Figure 4. The total mass loss of Fe_3O_4@PS and pure MNPs was determined to be 4.90% and 3.80%, respectively. Notably, similar peaks at 100, 214, 441, and 460 °C were observed in the DTGA profiles of both materials.

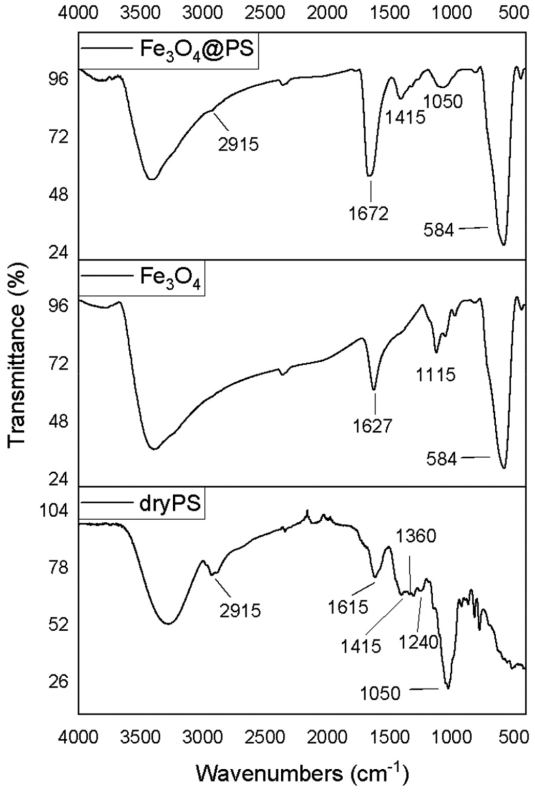

Figure 3. *FT-IR spectrum of dry pseudostem juice (dry PS), bare magnetite nanoparticles (F_3O_4), and the hybrid from the reaction of Fe_3O_4 and the PS juice*

The mass loss observed in the temperature range of 40 to 140 °C can be attributed to the evaporation of adsorbed water, a typical process observed in materials. The ranges of 170-270 °C and 400-560 °C correspond to the dehydroxylation process, as reported by Wu *et al*.[63] However, during the latter process, simultaneous decomposition of phytochemical compounds takes place. Interestingly, the DTGA plot of Fe_3O_4@PS exhibited a mass loss of 0.86% at 300-400 °C, indicating the volatilization of the organic fraction. This mass loss was compared with the DTGA plot of a dry PS sample, where a maximum mass loss of 15.10% was observed due to the presence of sodium and potassium components in the ash. Because PS juice

contains sodium and potassium as components of ashes[32] it is observed the mass loss is 15.10% maximum. The thermograms showed evidence of the reduction of Fe_3O_4 to Fe and FeO in the temperature range of 570-650 °C, with a maximum at 613 °C, as suggested by Rudolph *et al.*[64] At higher temperatures, no further decomposition was observed. These findings support the previous hypothesis that certain phytochemicals present in the PS act as capping agents during the surface modification of MNPs, influencing their thermal degradation behavior.

The results indicate that the Fe_3O_4@PS nanocomposite possesses distinctive thermal properties due to the presence of the phytochemicals, which can play a role in the stability and functionality of the composite material.

Electron microscopy images analysis

The nanoparticles were characterized using electron microscopy techniques. Scanning electron microscopy (SEM) was employed to investigate whether crystal microstructures of bulk magnetite were formed due to the ultrasound treatment. In Figure 5, no grain boundaries, terraces, or steps were observed, indicating that there was no significant growth of crystal domains at the expense of smaller nanoparticles through processes like Ostwald ripening or coalescence during the phytofunctionalization process.[61,65]

The cauliflower-like appearance of the Fe_3O_4@PS surface, as seen in Figure 5, suggests the presence of discrete nano-sized particles. This was further confirmed by transmission electron microscopy (TEM) images shown in Figure 6, which revealed a distribution of nanoparticles with nano-sized dimensions. The presence of organic capping at the surface of the nanoparticles likely contributes to the existence of Van der Waals forces, resulting in the aggregation of nanoparticles into clustered regions. Despite the predominant clustering, a detailed analysis of the TEM images enabled the determination of the size distribution of the nanoparticles, with an average diameter of 12.6 ± 3.17 nm, as depicted in Figure 7.

A comparison of these results with the findings of Venkateswarlu *et al.*[41] indicates that the Fe_3O_4@PS nanoparticles in this study were smaller. This difference can be attributed to the distinct synthesis routes employed in the two studies.

In conclusion, the process of phytofunctionalization under sonochemical treatment, following the synthesis of MNPs, leads to the formation of smaller nanoparticles. This study provides confirmation of the conservation in nanoparticle size achieved through the sonochemical-assisted phytofunctionalization process.

Chelating activity

Metal ions are a significant source of pollution in water resources and have detrimental effects on ecosystems. The increase in metal pollution is primarily attributed to anthropogenic activities.[66] Considering this, the development of novel materials such as Fe_3O_4@PS provides an opportunity to address the issue of metal ion contamination in water effluents. In this study, we investigated the potential capability of Fe_3O_4@PS to remove toxic metal ions from water, offering a promising approach for the remediation of contaminated water sources.

In order to evaluate the capture capacity of Cd(II) and Pb(II) ions from water, a chelating assay was conducted by comparing the metal concentrations before and after treatment with the Fe_3O_4@PS hybrid. The results indicated that the concentration of Cd(II) and Pb(II) in water decreased significantly following treatment with the nanocomposite, as shown in Figure 8. At a metal concentration of 10 ppm, the Fe_3O_4@PS hybrid demonstrated a remarkable metal withdrawal rate of 99.32% for Pb(II) and 87.78% for Cd(II). However, it should be noted that the capture efficiency decreases at higher metal concentrations, as the Fe_3O_4@PS hybrid reaches its saturation point.

The nanocomposite exhibited a good agreement with the Langmuir plot, as indicated by an R^2 value close to 1 (Figure 9).

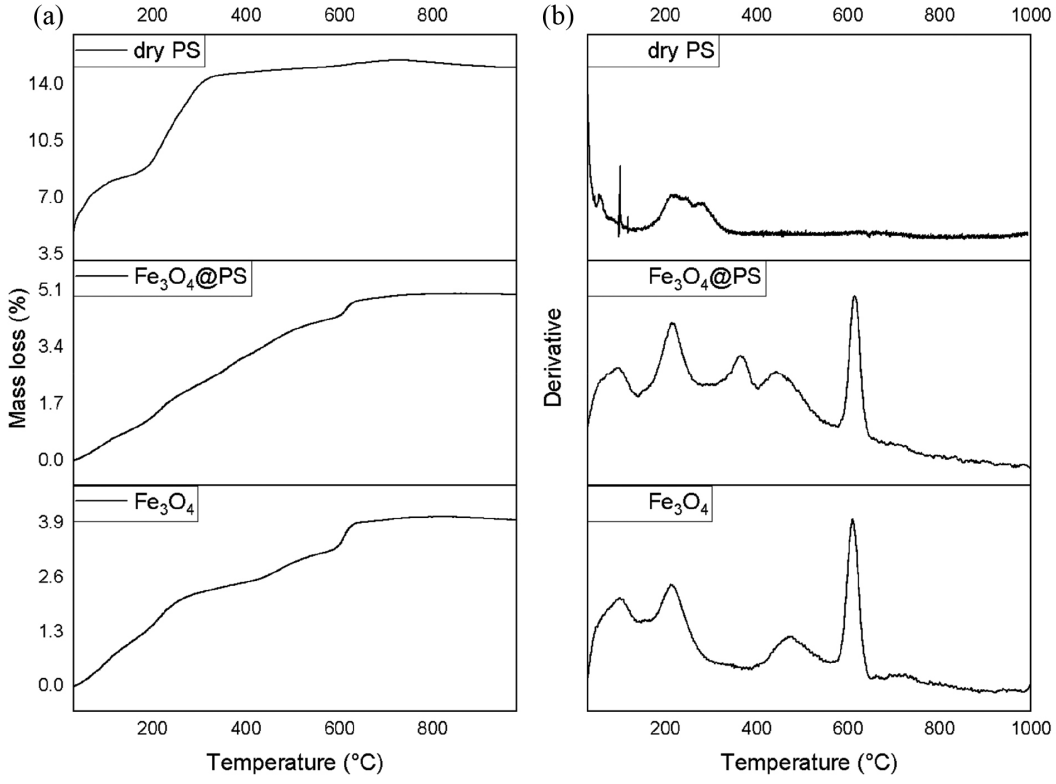

Figure 4. *Thermograms of samples of a dry PS sample, Fe_3O_4 MNPs, and Fe_3O_4@PS (a) and its derivative (b)*

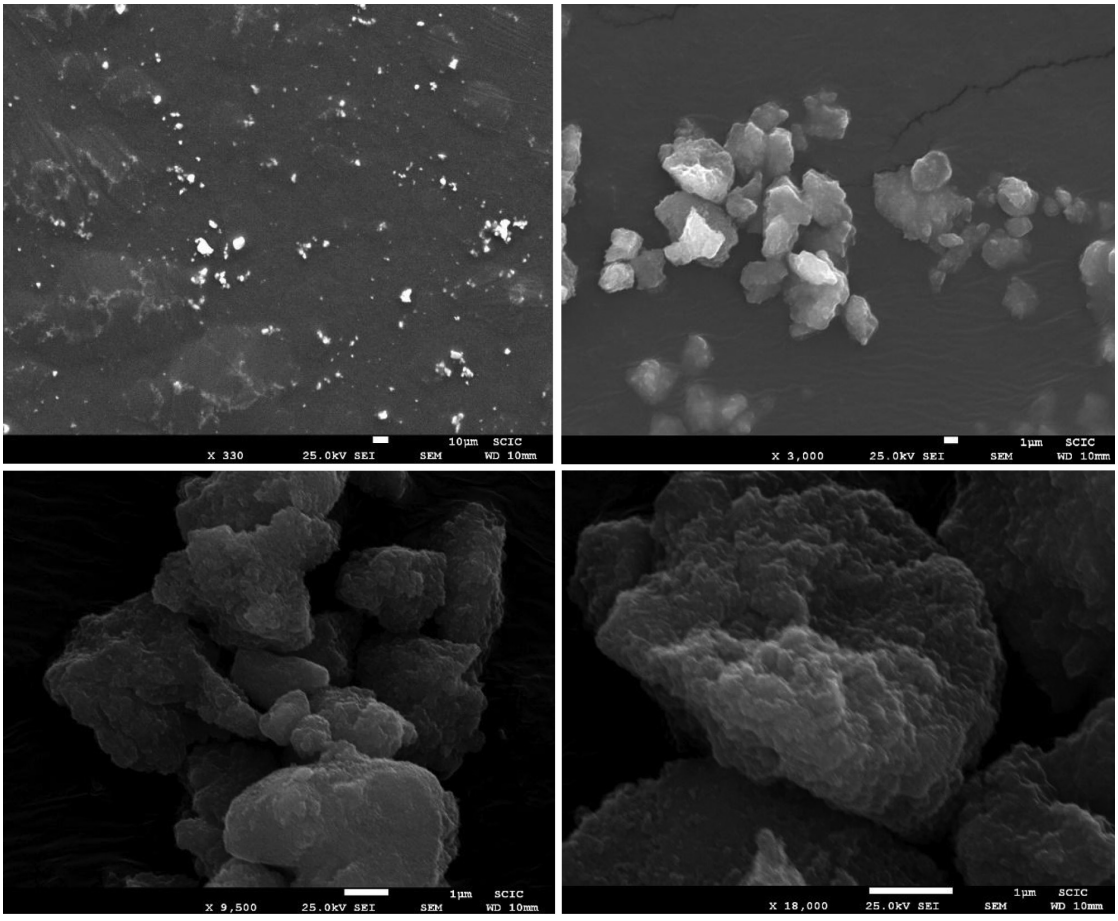

Figure 5. *SEM images of Fe_3O_4@PS*

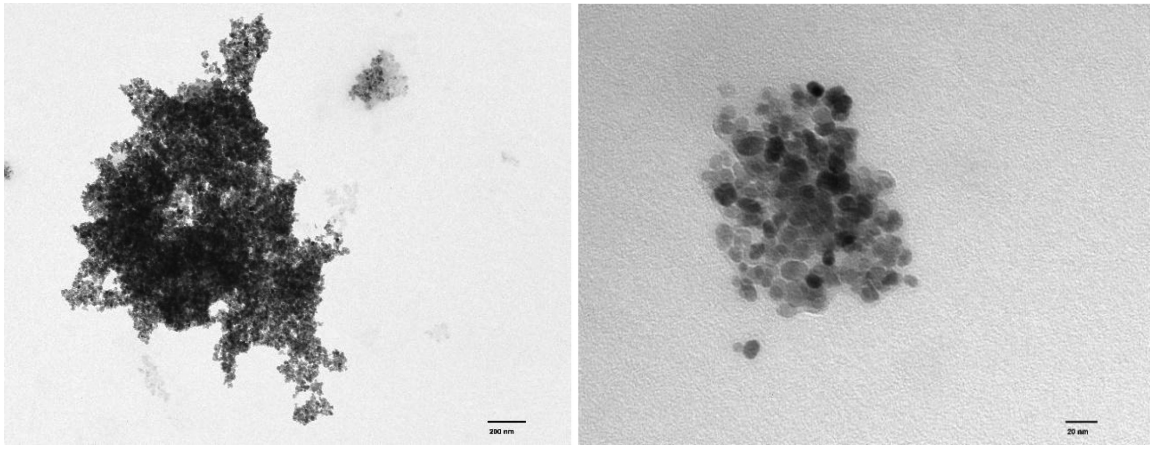

Figure 6. *TEM images of Fe_3O_4@PS*

This suggests the formation of a monolayer of the adsorbate on a homogeneous surface, indicating a favorable adsorption process.[50] The close alignment with the Langmuir isotherm model implies that the adsorption of the target species occurs on a single layer of active sites on the surface of the nanocomposite, leading to efficient and predictable adsorption behavior. It is important to note that the objective of this study was not to optimize specific conditions, but rather to demonstrate the chelating activity of the new material. The focus was on showcasing the potential of the synthesized material for effectively binding and removing heavy metals from aqueous solutions.

When comparing the adsorption capacity with literature exhibited, Fe_3O_4@PS showed a remarkably higher adsorption capacity (q_m) compared to the bio-based adsorbents listed in Table 3. What sets Fe_3O_4@PS apart is its simplicity in terms of not requiring complicated or exotic ligands such as PAMAM, as well as its straightforward synthesis process. Moreover, the nanostructured nature of Fe_3O_4@PS outperforms materials with microstructured tailoring, such as watermelon rind (WR). Another advantage of Fe_3O_4@PS is its ease of recovery using magnetic techniques, eliminating the need for additional filtration or centrifugation steps in the separation process. Overall, these factors contribute to the superior performance and practical applicability of Fe_3O_4@PS as an efficient adsorbent for metallic ions contaminants.

This exceptional capacity can be attributed to the multiple chelating points present on the surface of the MNPs, provided by

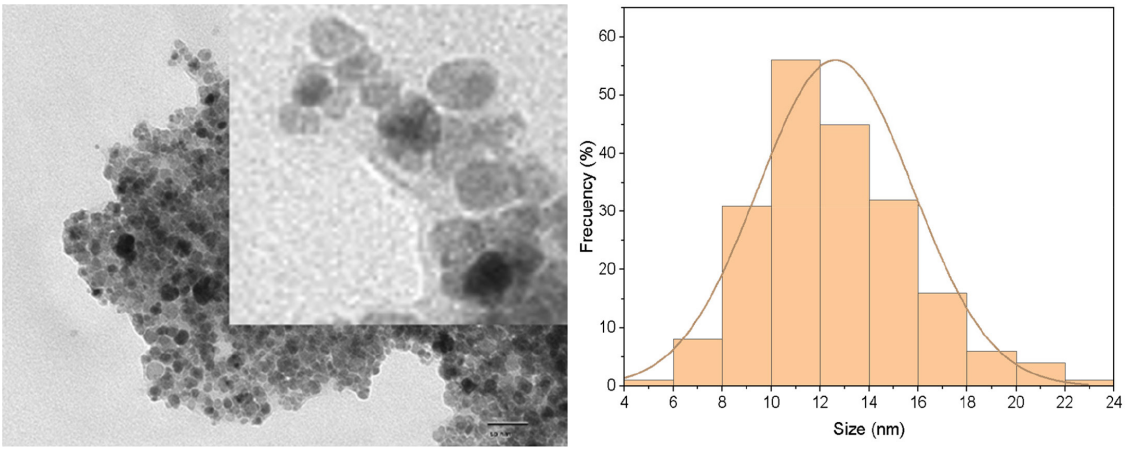

Figure 7. *Fe_3O_4@PS TEM image detail that shows the organic coating (light gray) surrounding the magnetite core (black and dark gray)*

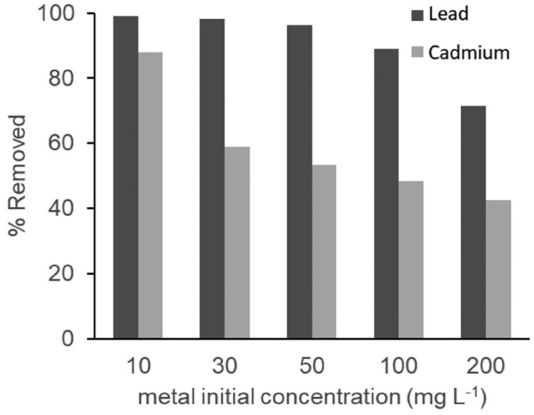

Figure 8. *The chelating activity of Fe_3O_4@PS*

the phytochemicals from PS, as well as the nano-size of the hybrid material. Taking into account that the phytochemicals from PS can have intrinsic chelating activity because of the bearing of phenolic and carbonyl compounds,[47,72] it is possible the adsorption of metal ions M^{2+} by coordination bonding. We think that the reason for the observed depletion of Cd(II) and Pb(II) concentrations is prompted by the organic cap provided by the PS to the MNPs since the negligible variation when treatment with bare MNPs was applied in a separate experiment. Furthermore, the nano-dimensional tailoring of the material offers a large surface area, providing ample active sites for the adsorption of metals dissolved in water. The increased surface area-to-volume ratio of the nanostructured material enhances its adsorption capacity, allowing for more efficient and effective removal of metals from aqueous solutions. This feature makes the material particularly suitable for applications in water treatment and remediation processes.

These findings further underscore the potential of Fe_3O_4@PS as an effective adsorbent for the efficient removal of Cd(II) and Pb(II) ions from water, particularly at lower metal concentrations. The exceptional adsorption capacity of Fe_3O_4@PS makes it a promising candidate for addressing water pollution issues associated with heavy metal contamination.

CONCLUSIONS

In conclusion, we have successfully synthesized a novel nanomaterial by combining magnetite nanoparticles (MNPs) with an organic phase derived from plantain pseudostem juice. The modification of the bare magnetite NPs through ultrasound treatment, known as phytofunctionalization, was successfully achieved. Although there was a slight reduction in the magnetic saturation, the superparamagnetic profile of the NPs remained largely unchanged. The resulting biobased nanomaterial exhibited nanoscale dimensions and demonstrated excellent dispersibility in water. This characteristic is particularly advantageous as it fulfills the requirements for effective dispersion, recovery, and redispersion of an adsorbent for water pollutants at room temperature. Overall, this innovative nanomaterial holds great potential as an efficient and environmentally friendly adsorbent for water remediation applications.

The study demonstrated that the post-synthesis method of functionalization (first synthesizing the MNPs and then modifying the surface with PS) resulted in the successful production of superparamagnetic nanoparticles. Importantly, the surface modification process did not require any additional solvents or water, contributing to the overall greenness of the approach. Additionally,

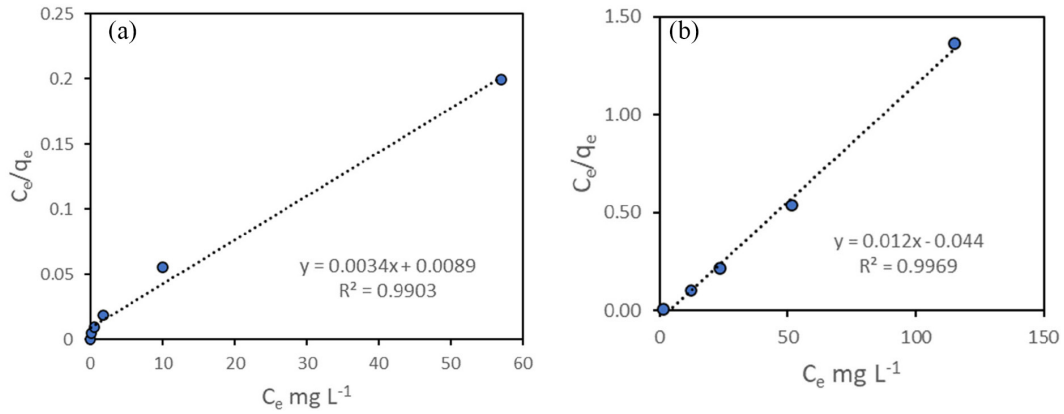

Figure 9. *Isotherm Langmuir plot for Fe_3O_4@PS as adsorbent in contaminated water: (a) Pb(II) and (b) Cd(II)*

Table 3. Parameters of bio-based materials in adsorption of heavy metals

Nanomaterial	Bio-based material description	Metal	C_0 (mg L^{-1})	pH	Adsorbent (g L^{-1})	q_m (mg g^{-1})	Removal (%)
Fe_3O_4 MNRs[56]	Magnetic nanorods using *Punica granatum* rind extract decorated with MNPs	Pb(II)	20	5	1.0	46.18	96.68
Iota-Carrageenan/ PAMAM[67]	Iota Carrageenan; Iota-Carrageenan cross-linked with Olyamidoamine hyperbranched polymer generation 1 (PAMAM)	Cd(II)	20	2	1.0	*	98.00
Raw eggshell[68]	Dry hen eggshell	Pb(II) Cd(II)	40	5.5	10.0	277.70 13.62	99.55 75.00
Raw sugarcane[68]	Wash and dry sugarcane bagasse	Pb(II) Cd(II)	40	5.5	10.0	31.45 19.49	80.00 85.25
Nanoadsorbent of Oryza sativa husk[69]	Alkali treatment, bleaching, acid hydrolysis, centrifugation, ultrasonication and stirring of biomaterial	Pb(II)	10	8	12.0	6.10	91.90
Nanostructured clay[70]	Sample collected from Siahkalahan Mine (Kerman, Iran)	Pb(II)	100	5	10	36.2	80.00
Watermelon rind (WR)[71]	Dried and crushed WR. Particles smaller than 180 μm were sectioned	Cd(II)	100	7	5	102	81.00
Fe_3O_4@PS	This work	Pb(II) Cd(II)	10	7	0.5	294.1 83.33	99.32 87.78

*Freundlich model applied do not predicts maximum adsorption capacity.

ultrasound was utilized as a means of facilitating the surface modification process, further enhancing the eco-friendliness of the method.

To the best of our knowledge, this study represents the first utilization of phytochemicals derived from plantain pseudostem (*Musa paradisiaca* var. Domico hartón) for the modification of MNPs. Furthermore, it is the first instance where pseudostem juice has been incorporated into nanoparticles, particularly for advanced applications such as the removal of toxic metals from water. The successful demonstration of their efficacy in removing toxic metals highlights their potential for addressing environmental challenges and offers a promising solution for water decontamination processes. While optimization of conditions can be a valuable future direction, the primary aim of this study was to establish the chelating capabilities of the developed material and highlight its applicability for metal removal.

Finally, this innovative approach significantly broadens the potential utilization of local bioresources and serves as a starting point for their application in various fields. These fields encompass bioremediation, drug delivery systems, elimination of emerging pollutants, and others. The successful incorporation of plantain pseudostem-derived phytochemicals into nanoparticles not only showcases their versatility but also new possibilities emerge for addressing environmental and biomedical challenges.

ACKNOWLEDGEMENTS

The authors would like to express their gratitude to Cesar Augusto Angulo Pachón from Universitat Jaume I for his invaluable assistance in obtaining the results presented in this study. Secondly, we extend our thanks to Universidad del Tolima for providing financial support for this research. The authors also acknowledge the members of the QUAPE laboratory for their valuable contributions to the project. Special thanks are extended to Camilo López "Milo" from "La colombina" farm for his valuable assistance in the cultivation and harvest of organic plantains, as well as for kindly supplying the pseudostems and contributing to the photography in Figure 1. Lastly, the authors would like to thank Sandra Patricia Alzate for her guidance and support in editing the english version of the project.

REFERENCES

1. Bruckmann, F. S.; Viana, A. R.; Tonel, M. Z.; Fagan, S. B.; Garcia, W. J. S.; de Oliveira, A. H.; Dorneles, L. S.; Mortari, S. R.; da Silva, W. L.; da Silva, I. Z.; Rhoden, C. R. B.; *Environ. Sci. Pollut. Res.* **2022**, *29*, 70413. [Crossref]
2. Khan, I.; Saeed, K.; Khan, I.; *Arabian J. Chem.* **2019**, *12*, 908. [Crossref]
3. Neouze, M. A.; Schubert, U.; *Monatshefte für Chemie - Chemical Monthly* **2008**, *139*, 183. [Crossref]
4. Mishra, S.; Ganapathy, M.; Padmanabhan, P.; Gulyás, B.; Thiruppathi, R.; *Advanced Science* **2017**, *4*, 1600279. [Crossref]
5. Estelrich, J.; Escribano, E.; Queralt, J.; Busquets, M. A.; *Int. J. Mol. Sci.* **2015**, *16*, 8070. [Crossref]
6. Yang, B.; Ouyang, D.; Huang, Z.; Ren, X.; Zhang, H.; Choy, W. C. H.; *Adv. Funct. Mater.* **2019**, *29*, 1902600. [Crossref]
7. Gour, A.; Jain, N. K.; *Artif. Cells, Nanomed., Biotechnol.* **2019**, *47*, 844. [Crossref]
8. Hussain, I.; Singh, N. B.; Singh, A.; Singh, H.; Singh, S. C.; *Biotechnol. Lett.* **2016**, *38*, 545. [Crossref]
9. Rana, A.; Yadav, K.; Jagadevan, S.; *J. Cleaner Prod.* **2020**, *272*, 122880. [Crossref]
10. Bala, A.; Rani, G.; *Int. Nano Lett.* **2020**, *10*, 159. [Crossref]
11. Küünal, S.; Rauwel, P.; Rauwel, E. In *Emerging Applications of Nanoparticles and Architectural Nanostructures: Current Prospects and Future Trends*; Barhoum, A.; Makhlouf, A. S. H., eds.; Elsevier: Amsterdam, 2018, p. 411-446. [Crossref]
12. Jadoun, S.; Arif, R.; Jangid, N. K.; Meena, R. K.; *Environ. Chem. Lett.* **2021**, *19*, 355. [Crossref]
13. Alamdari, S.; Ghamsari, M. S.; Lee, C.; Han, W.; Park, H. H.; Tafreshi, M. J.; Afarideh, H.; Ara, M. H. M.; *Appl. Sci.* **2020**, *10*, 3620. [Crossref]
14. Ahmed, A.; Usman, M.; Liu, Q. Y.; Shen, Y. Q.; Yu, B.; Cong, H. L.; *Ferroelectrics* **2019**, *549*, 61. [Crossref]
15. Paulkumar, K.; Gnanajobitha, G.; Vanaja, M.; Rajeshkumar, S.; Malarkodi, C.; Pandian, K.; Annadurai, G.; *Sci. World J.* **2014**, *2014*, 1. [Crossref]
16. Benakashani, F.; Allafchian, A.; Jalali, S. A. H.; *Green Chem. Lett. Rev.* **2017**, *10*, 324. [Crossref]
17. Padil, V. V. T.; Wacławek, S.; Černík, M.; *Ecol. Chem. Eng. S* **2016**, *23*, 533. [Crossref]

18. Nava, O. J.; Soto-Robles, C. A.; Gómez-Gutiérrez, C. M.; Vilchis-Nestor, A. R.; Castro-Beltrán, A.; Olivas, A.; Luque, P. A.; *J. Mol. Struct.* **2017**, *1147*, 1. [Crossref]
19. Rautela, A.; Rani, J.; Das, M. D.; *J. Anal. Sci. Technol.* **2019**, *10*, 1. [Crossref]
20. Jaffri, S. B.; Ahmad, K. S.; *Rev. Inorg. Chem.* **2018**, *38*, 127. [Crossref]
21. Rhoden, C. R. B.; Bruckmann, F. S.; Salles, T. R.; Kaufmann Junior, C. G.; Mortari, S. R.; *Journal of Water Process Engineering* **2021**, *43*, 102262. [Crossref]
22. Bruckmann, F. S.; Viana, A. R.; Lopes, L. Q. S.; Santos, R. C. V.; Muller, E. I.; Mortari, S. R.; Rhoden, C. R. B.; *J. Inorg. Organomet. Polym. Mater.* **2022**, *32*, 1459. [Crossref]
23. Masuku, M.; Ouma, L.; Pholosi, A.; *Environ. Nanotechnol., Monit. Manage.* **2021**, *15*, 100429. [Crossref]
24. Mohammadzadeh, M.; Leiviskä, T.; *Ind. Crops Prod.* **2023**, *195*, 116491. [Crossref]
25. Nayak, A.; Bhushan, B.; Kotnala, S.; *J. Hazard. Mater. Adv.* **2023**, *10*, 100308. [Crossref]
26. Nematollahzadeh, A.; Babapoor, A.; Mousavi, S. M.; Nuri, A.; *Mater. Chem. Phys.* **2021**, *262*, 124266. [Crossref]
27. Ekinci, S.; İlter, Z.; Ercan, S.; Çınar, E.; Çakmak, R.; *Heliyon* **2021**, *7*, e06600. [Crossref]
28. Ahmad, N.; Arsyad, F. S.; Royani, I.; Lesbani, A.; *Results Chem.* **2022**, *4*, 100629. [Crossref]
29. Reuters, https://www.reuters.com/article/colombia-bananas-idINL1N2M71T5, accessed in August 2023.
30. Parra-Ramírez, D.; Solarte-Toro, J. C.; Cardona-Alzate, C. A.; *Waste Biomass Valorization* **2019**, *11*, 3161. [Crossref]
31. Phirke, N. V.; Patil, R. P.; Chincholkar, S. B.; Kothari, R. M.; *Resour., Conserv. Recycl.* **2001**, *31*, 347. [Crossref]
32. Vargas, L.; Yepes, P.; Guarnizo, A.; *Rev. Cienc.* **2013**, *17*, 47. [Crossref]
33. Guarnizo, A.; Martínez, P.; Pinzón, M. L.; *Bistua* **2012**, *1*, 39. [Link] accessed in August 2023
34. Tsamo, C. V. P.; Herent, M. F.; Tomekpe, K.; Emaga, T. H.; Quetin-Leclercq, J.; Rogez, H.; Larondelle, Y.; Andre, C.; *Food Chem.* **2015**, *167*, 197. [Crossref]
35. Saravanan, K.; Aradhya, S. M.; *J. Agric. Food Chem.* **2011**, *59*, 3613. [Crossref]
36. Santos, J. R. U.; Bakry, F.; Brillouet, J. M.; *Biochem. Syst. Ecol.* **2010**, *38*, 1010. [Crossref]
37. Rahim, M. A.; Kristufek, S. L.; Pan, S.; Richardson, J. J.; Caruso, F.; *Angew. Chemie* **2019**, *58*, 1904. [Crossref]
38. Uchenna, A. P.; Charity, O. N. U.; Bene, A.; *Recent Pat. Food, Nutr. Agric.* **2019**, *10*, 140. [Crossref]
39. Bankar, A.; Joshi, B.; Kumar, A. R.; Zinjarde, S.; *Colloids Surf., A* **2010**, *368*, 58. [Crossref]
40. Ibrahim, H. M. M.; *J. Radiat. Res. Appl. Sci.* **2015**, *8*, 265. [Crossref]
41. Venkateswarlu, S.; Rao, Y. S.; Balaji, T.; Prathima, B.; Jyothi, N. V. V.; *Mater. Lett.* **2013**, *100*, 241. [Crossref]
42. Boo, H. O.; Hwang, S. J.; Bae, C. S.; Park, S. H.; Heo, B. G.; Gorinstein, S.; *Ind. Crops Prod.* **2012**, *40*, 129. [Crossref]
43. Galvão, M. A. M.; de Arruda, A. O.; Bezerra, I. C. F.; Ferreira, M. R. A.; Soares, L. A. L.; *Braz. Arch. Biol. Technol.* **2018**, *61*, 1. [Crossref]
44. Baruwati, B.; Polshettiwar, V.; Varma, R. S.; *Tetrahedron Lett.* **2009**, *50*, 1215. [Crossref]
45. Armelles, G.; Cebollada, A.; García-Martín, A.; González, M. U.; *Adv. Opt. Mater.* **2013**, *1*, 10. [Crossref]
46. Abdelhakim, S.; Rima, B.; Abdelouahab, B.; *Journal of Ecological Engineering* **2019**, *20*, 116. [Crossref]
47. Sánchez-Vioque, R.; Polissiou, M.; Astraka, K.; Pascual, M. M.; Tarantilis, P.; Herraiz-Peñalver, D.; Santana-Méridas, O.; *Ind. Crops Prod.* **2013**, *49*, 150. [Crossref]
48. Wong, F. C.; Yong, A. L.; Ting, E. P. S.; Khoo, S. C.; Ong, H. C.; Chai, T. T.; *Iran. J. Pharm. Res.* **2014**, *13*, 1409. [Link] accessed in August 2023
49. Baird, R. B.; Eaton, A. D.; Rice, E. W.; *Standard Methods for the Examination of Water and Wastewater*, 23rd ed.; American Water Works Association: Washington, 2017.
50. Osmari, T. A.; Gallon, R.; Schwaab, M.; Coutinho, E. B.; Severo, J. B.; Pinto, J. C.; *Adsorpt. Sci. Technol.* **2013**, *31*, 433. [Crossref]
51. Miller, J. S.; *Mater. Today* **2014**, *17*, 224. [Crossref]
52. Guarnizo, A.; Angurell, I.; Muller, G.; Llorca, J.; Seco, M.; Rossell, O.; Rossell, M. D.; *RSC Adv.* **2016**, *6*, 68675. [Crossref]
53. Veisi, H.; Karmakar, B.; Tamoradi, T.; Tayebee, R.; Sajjadifar, S.; Lotfi, S.; Maleki, B.; Hemmati, S.; *Sci. Rep.* **2021**, *11*, 1. [Crossref]
54. Sathishkumar, G.; Logeshwaran, V.; Sarathbabu, S.; Jha, P. K.; Jeyaraj, M.; Rajkuberan, C.; Senthilkumar, N.; Sivaramakrishnan, S.; *Artif. Cells, Nanomed., Biotechnol.* **2017**, *46*, 589. [Crossref]
55. Fard-Fini, S. A.; Salavati-Niasari, M.; Ghanbari, D.; *Spectrochim. Acta, Part A* **2018**, *203*, 481. [Crossref]
56. Venkateswarlu, S.; Kumar, B. N.; Prathima, B.; SubbaRao, Y.; Jyothi, N. V. V.; *Arabian J. Chem.* **2019**, *12*, 588. [Crossref]
57. Elrhman, H. M. A.; *Results Mater.* **2020**, *8*, 100138. [Crossref]
58. Hou, D. Z.; Ling, P.; Zhu, Y.; Ouyang, Y. M.; Karmakar, B.; *Arabian J. Chem.* **2022**, *15*, 104219. [Crossref]
59. Tang, X.; Li, X.; Sun, Z.; *Arabian J. Chem.* **2022**, *15*, 103816. [Crossref]
60. Stoia, M.; Istratie, R.; Păcurariu, C.; *J. Therm. Anal. Calorim.* **2016**, *125*, 1185. [Crossref]
61. Karade, V. C.; Waifalkar, P. P.; Dongle, T. D.; Sahoo, S. C.; Kollu, P.; Patil, P. S.; Patil, P. B.; *Mater. Res. Express* **2017**, *4*, 1. [Crossref]
62. Khalil, M. I.; *Arabian J. Chem.* **2015**, *8*, 279. [Crossref]
63. Wu, C. X.; Wen, S. Z.; Yan, L. K.; Zhang, M.; Ma, T. Y.; Kan, Y. H.; Su, Z. M.; *J. Mater. Chem. C* **2017**, *5*, 4053. [Crossref]
64. Rudolph, M.; Erler, J.; Peuker, U. A.; *Colloids Surf., A* **2012**, *397*, 16. [Crossref]
65. Hansen, T. W.; Delariva, A. T.; Challa, S.; *Acc. Chem. Res.* **2013**, *46*, 1720. [Crossref]
66. Vareda, J. P.; Valente, A. J. M.; Durães, L.; *J. Environ. Manage.* **2019**, *246*, 101. [Crossref]
67. Abdellatif, F. H. H.; Abdellatif, M. M.; *Cellulose* **2020**, *27*, 441. [Crossref]
68. Harripersadth, C.; Musonge, P.; Makarfi Isa, Y.; Morales, M. G.; Sayago, A.; *S. Afr. J. Chem. Eng.* **2020**, *34*, 142. [Crossref]
69. Kaur, M.; Kumari, S.; Sharma, P.; *Biotechnol. Rep.* **2020**, *25*, e00410. [Crossref]
70. Ghasemi, H.; Afshang, M.; Gilvari, T.; Aghabarari, B.; Mozaffari, S.; *Results in Surfaces and Interfaces* **2023**, *10*, 100097. [Crossref]
71. Wang, Q.; Wang, Y.; Yuan, L.; Zou, T.; Zhang, W.; Zhang, X.; Zhang, L.; Huang, X.; *Chem. Eng. J. Adv.* **2022**, *12*, 100393. [Crossref]
72. Lakey-Beitia, J.; Burillo, A. M.; La Penna, G.; Hegde, M. L.; Rao, K. S.; *J. Alzheimer's Dis.* **2021**, *82*, S335. [Crossref]